IOP Conf. Series: Materials Science and Engineering **381** (2018) 012132 doi:10.1088/1757-899X/381/1/012132

Detection of Ammonia Using Logarithmic-Transformed Wavelength Modulation Spectrum

Menglong Cong[a,*] and Dandan Sun[b]

College of Physics and Electronic Information, Inner Mongolia University for the Nationalities, No.22, Huolinhe street, Tongliao, Inner Mongolia, P. R. China
E-mail: [a]congml@163.com, [b]myflarry@163.com

Abstract. Conventional wavelength modulation spectroscopy is improved by logarithmic-transformed data processing and differential detection for trace gas sensing. The optic intensity modulation is isolated from the gas absorption induced laser power attenuation via the logarithmic-transformation, and then it is balanced out by differential detection. The theory is validated by the detection of P(6) NH3-absorption line belonging to the ν3 + ν4 combination band in a stainless tube with effective path length of 24.5 cm, under room temperature (296 K) and atmospheric pressure (1.01e5 Pa). The second harmonic is recovered while the residual amplitude modulation and distortion of harmonic are eliminated.

1. Introduction

Infrared absorption spectroscopy, characterized with benefits of high sensitivity, good selectivity, remote and non-destructive sensing, is very popular for trace gas detection [1]. Sensors based on this technique have been spread to various applications such as space exploration [2], combustion diagnostics [3], and atmosphere monitoring, chemistry and process control [4]. As a useful light source for these applications, the near-infrared diode laser features with low cost, compact structure and easily scanned wavelength [5].

Wavelength modulation spectroscopy (WMS) [6] is introduced to improve the sensitivity. The lasing wavelength is modulated to produce harmonics of the absorption coefficient. Consequently, the detection is transferred to higher frequency where the flicker noise is weaker. Accompany with the wavelength modulation, the optical intensity modulation (IM), which is the root of residual amplitude modulation (RAM) and distortion of harmonic [7], occurs inevitably. The second harmonic, named WMS-2*f* [8], is often studied for its relatively strong amplitude. In order to obtain the absolute concentration or temperature, the 2*f* signal must be calibrated to a known mixture and condition (or a direct measurement of absorption) [9]. The fluctuation of laser intensity raises a rigorous demand on the real-time performance of calibration. For most real-world environments and field-deployable sensors the real-time calibration is difficult and impractical, and may involve the need for additional equipment or complexity of sensor. The calibration could be exempt by normalizing the second harmonic with the first harmonic [10]. After the normalization, their common variations, such as the optical intensity fluctuation, detection phase, optic-electronic conversion efficiency and transmittance, are all removed. This calibration free method is termed as WMS-2*f* /1*f* [11]. Regrettably, the increasing amplitude of WMS-2*f* /1*f* with the gas concentration is nonlinear, and the laser characterization is a little intricate.

In the present paper, a specific way called logarithmic-transformed WMS-2*f* is proposed to cope with the intricate characterization of probe laser and nonlinear variation of harmonic amplitude. Firstly, the experimental apparatus is sketched in Section 2. The system is based upon a distributed-feedback diode laser operating at 2.005 μm, in coincidence with the strong *P*(6) absorption line of NH_3 belonging to the

$v3 + v4$ combination band [12], with an intensity factor of 7.703×10^{-21} cm/molecule, as recorded in HITRAN database [13]. Then, the basic theory of logarithmic-transformed WMS-2*f* is described in Section 3. Absolute magnitude of 2*f* signal is calculated using the root-sum square of the harmonic vectors. The expression shows that the peak is only determined by gas concentration under the given conditions of effective optical path, referenced amplitude and spectral parameters. Finally, experimental results are listed in Section 4. The in-phase vector of WMS-2*f* is measured for different modulation index to study the effects of IM on curve shape and RAM. Dependence of the WMS-2*f* /1*f* and logarithmic-transformed WMS-2*f* on the mole fraction of NH_3 are analyzed and compared. Continuous measurements for different gas concentrations are repeated 20 times during 240 hours to evaluate the repeatability.

2. Experimental section

Fig.1 shows the experimental setup of the absorption spectroscopy based gas analyzer. The gas cell is made of a stainless tube with effective path length of 24.5 cm. Three type K thermocouples are attached to the middle and both end faces to monitor the gas temperature. A distributed feedback (DFB) diode laser is packaged in a commercial laser mount with build-in thermo-electric cooler and thermistor (Mitsubishi, FU-68PDF-V510). It delivers coherent radiation up to 10 mW, on a single mode at 2.005 μm, with a threshold current of 22 mA at working temperature of 310 K. The current and temperature of the laser are properly adjusted in order to detect the *P*(6) NH_3-absorption line (corresponding to center wavenumber of 4986.995500 cm^{-1}) via a low-noise laser current supply (Newport, Model 500B) and a high-precision laser temperature controller (ILX, Model LDT-5900C).

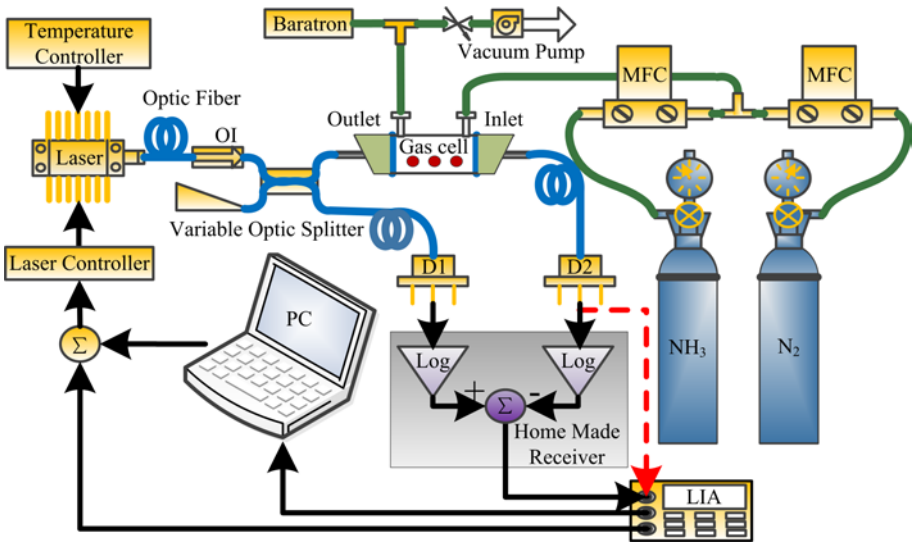

Figure 1. Schematic diagram of the experimental setup (MFC: mass flow controller, OI: optical isolator and LIA: lock-in amplifier).

Scanning of the absorption spectral is achieved by applying a 10 Hz triangular wave to the input of the laser current controller. A 10 kHz sinusoidal generated from the lock-in amplifier is added to modulate the wavelength. The laser is fiber coupled to an optical isolator to avoid the optical feedback scattering of the cell, and then divided into a sampling beam and a referenced beam by a fiber splitter. After a single pass through the gas volume under test, the sampling beam is guided onto an InGaAs photo diode with 1 mm^2 active area. Meanwhile, an identical photo diode is placed on the referenced beam to track the IM. In a homemade receiver, the currents delivered by these photo diodes are logarithm converted to voltages, and then the sampling voltage is subtracted from the referenced one. The output of the receiver is sent to the lock-in amplifier and demodulated at twice the modulation frequency to yield a 2*f* signal, and digitized via a 12 bit A/D-converter to a PC programmed with LABVIEW.

3. Basic theory of logarithmic-transformed WMS-2f

According to Beer–Lambert's law, light passes through a uniform gas medium is attenuated by the absorption. The transmitted intensity, I_t, and the incident intensity, I_0, is related by

$$I_t = I_0 \times \exp[-S(T)g(\nu)NL] \tag{1}$$

where $S(T)$ is the strength of absorption line at temperature T, N is the number density of molecules, L is the effective optic path, and $g(\nu)$ is the function of instantaneous wavenumber ν for depicting the line shape. Under room temperature and atmosphere pressure, $g(\nu)$ is simplified to Lorentz function as

$$g_L(\nu) = \frac{1}{\pi\Delta\nu_L} \times \frac{1}{1+\left(\frac{\nu-\nu_0}{\Delta\nu_L}\right)^2} \tag{2}$$

where ν_0 is the resonance frequency of the absorption line and $\Delta\nu_L$ is the half width at half maximum (HWHM) which is calculated by

$$\Delta\nu_L = P\left[\left(1-x_{\mathrm{NH3}}\right)\Gamma_{\mathrm{N2}} + x_{\mathrm{NH3}}\Gamma_{\mathrm{NH3}}\right] \tag{3}$$

In Eq. 3, x_{NH3} is the mole fraction of NH_3 under the total pressure P, and Γ_{N2} and Γ_{NH3} represent the N_2-broadening coefficient and self-broadening coefficient of NH_3, which could be obtained from either direct absorption spectroscopy or HITRAN database.

The injection current of diode laser is tuned by a triangular waveform to ramp the average lasing wavenumber ν_a back and forth. Meanwhile, ν_a is modulated by a sinusoid with f_c the frequency and k the modulation index:

$$\nu(t) = \nu_a + k\Delta\nu_L \cos\left(2\pi f_c t\right) \tag{4}$$

Following with the modulation of wavenumber, the laser intensity is inevitably modulated, and the instantaneous intensity $I_0(t)$ could be written as

$$I_0(t) = I_a[1 + \xi_1 \cos\left(2\pi f_c t + \alpha\right) + \xi_2 \cos(4\pi f_c t + \beta)] \tag{5}$$

where I_a is the intensity at wavenumber ν_a, ξ_1 represents the normalized amplitude of the linear IM with the phase shift α, and ξ_2 represents the normalized amplitude of the nonlinear IM with the phase shift β. The sampling current, $i_s(t)$, and the referenced current, $i_r(t)$, is expressed by

$$\begin{aligned} i_s(t) &= K_s I_0(t)\exp[-S(T)g_L(\nu)NL], \\ i_r(t) &= K_r I_0(t). \end{aligned} \tag{6}$$

In Eq. 6, K_s and K_r are gains of the sampling beam and referenced beam, which account for the splitting ratio, transmittance and photodetector responsibility. Both of the currents are logarithm transformed, and their difference is exported:

$$i_d(t) = \ln[i_r(t)] - \ln[i_s(t)] = \ln\left(K_r / K_s\right) + S(T)g_L(\nu)NL \tag{7}$$

Resulting from the modulation of wavenumber, $g_L(\nu)$ becomes a periodic even function in $2\pi f_c t$, and can be expanded to Fourier Series follows

$$g_L[\nu(t)] = g_L[\nu_a + k\Delta\nu_L\cos(2\pi f_c t)] = \sum_{m=0}^{\infty} C_m(\nu_a, k, \Delta\nu_L)\cos(2m\pi f_c t) \tag{8}$$

with $C_m(\nu_a, k, \Delta\nu_L)$ the mth-order harmonic:

$$\begin{aligned} C_0(\nu_a, k, \Delta\nu_L) &= \frac{1}{2\pi}\int_{-\pi}^{+\pi} g_L(\nu_a + k\Delta\nu_L\cos\theta)\mathrm{d}\theta, \\ C_m(\nu_a, k, \Delta\nu_L) &= \frac{1}{\pi}\int_{-\pi}^{+\pi} g_L(\nu_a + k\Delta\nu_L\cos\theta)\cos(m\theta)\mathrm{d}\theta. \end{aligned} \tag{9}$$

According to Eq. 3 and Eq. 9, C_2 is simulated from the $P(6)$ line of NH_3 for different k values (0.6, 2.0 and 2.8). Fig. 2 illustrates the results versus the average wavenumber v_a in the range of 4986.4 cm^{-1} to 4987.6 cm^{-1}. Spectral parameters (Γ_{N2}, Γ_{NH3} and v_0) are obtained from the HITRAN database. Other parameters involved in simulation are x_{NH3} = 1%, P = 1.01×10^5 Pa and T = 296 K. No matter what the k is, the profile is symmetric with respect to resonance absorption frequency v_0. When v_a is tuned to be overlap with v_0, the peak of C_2, denoted as C_{2p}, is reached. Fig. 3 shows the simulated C_{2p} as a function of the modulation index k for different line shapes (Lorentzian, Voigt, and Gaussian). Though the variation depends slightly on line-shape functions, the k correspond to the maximum of C_{2p} are 2.2 without any exception.

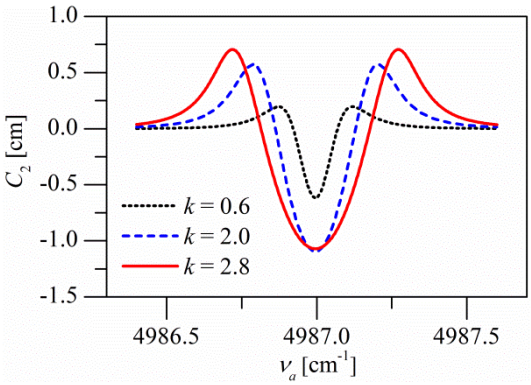

Figure 2. The calculated C_2 as a function of v_a for the P (6) line of NH_3 near 4986.995500 cm^{-1}; T = 296 K, P = 1.01×10^5 Pa and x_{NH3} = 1% diluted by N_2.

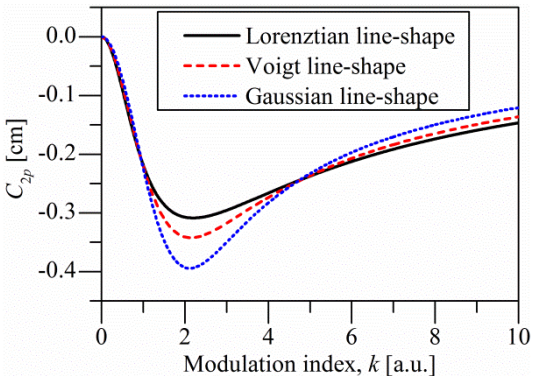

Figure 3. The calculated C2p for Lorentzian, Voigt, and Gaussian line shape as a function of modulation index, k, at the P (6) line of NH3 near 4986.995500 cm-1.

4. Results and Discussion

For WMS-2f/1f detection, the referenced beam and the following logarithmic-transformation stage are disabled. The in-phase vector of 2f signal, X_2, is output from the channel X of the lock-in amplifier. The reference phase of lock-in amplifier is carefully adjusted to maximize the amplitude of X_2. Fig. 4 illustrates the curves of X_2 for 1% NH_3 at three different modulation index, 0.6, 2.0 and 2.8. For smaller modulation index (k = 0.6), the IM could be negligible, and the waveform is dominated by C_2, which shows a strong single peak and two weak wing lobes lying on both sides of it. With the increasing of k (k = 2.0), the IM becomes evident, and the curve is seriously distorted by the linear terms of IM, which lead to the asymmetry of wings and the broadening of peak. Finally, when k is big enough (k = 2.8), the peak is about to be surpassed by the wing.

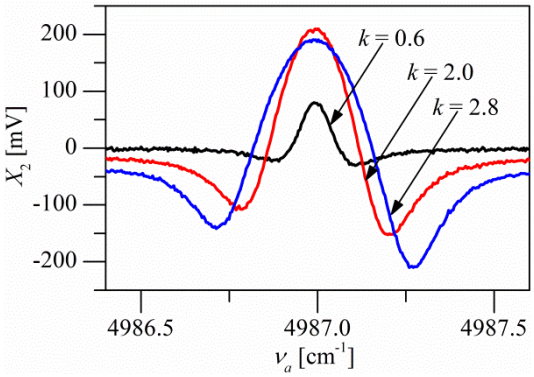

Figure 4. The in-phase vector of 2*f* signal, X_2, versus the average wavenumber, ν_a, for different modulation index, 0.6, 2.0 and 2.8; T = 296 K, P = 1.01×10^5 Pa, L = 24.5 cm and x_{NH3} = 1%.

In Fig. 5, the referenced beam and the logarithmic-transformation are enabled to deal with the RAM and distortion of WMS-2*f*/1*f*. Absolute magnitude of logarithmic-transformed WMS-2*f* is measured with 0.2%, 0.5% and 1% NH_3. When the peak is maximized by deliberately tuning the amplitude of modulated sinusoid, a modulation index *k* of 2.2 is confirmed naturally. The concentration-independent DC bias, which is brought by the RAM, is weakened to approximately zero, and the distortion has not been found.

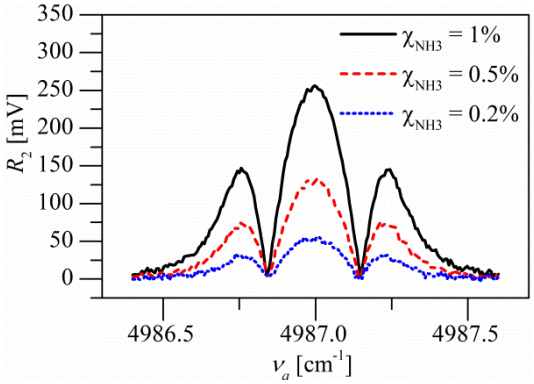

Figure 5. The absolute magnitude of logarithmic-transformed WMS-2*f* versus ν_a, for 1%, 0.5%, and 0.2% NH_3.

5. Summary

This work has demonstrated that WMS could be perfectly combined with logarithmic-transformed data processing and differential detection for gas sensing. The synthetic strategy has shown the superiorities in nulling the RAM and distortion of harmonics. The RAM is eliminated from the root, thus the optimum modulation index is easily confirmed. Unlike the general sense of differential detection which is sensitive to the asymmetry of the beams, the setup used here is immune from this problem. Gas mole fraction could be calculated directly from the peak value of harmonic, and the on-site calibration using a known mixture or operating condition is no longer needed. Compared with WMS-2f /1f detection, though they are both calibration free, the mathematic model in this research is independent of laser parameters.

6. Acknowledgement

This research was financially supported by the “Science research project of Inner Mongolia University for the Nationalities”. (No. NMDYB17163)

7. References

[1] M. Nikodem, G. Wysocki, Chirped laser dispersion spectroscopy for remote open-path trace-gas sensing, Sensors 12 (2012) 16466-16481.
[2] R. Gaudiuso, M. Dell'Aglio, O. D. Pascale, G. S. Senesi, A. D. Giacomo, Laser induced breakdown spectroscopy for elemental analysis in environmental, cultural heritage and space applications: a review of methods and results, Sensors 10 (2010) 7434-7468.
[3] W. Zeller, L. Naehle, P. Fuchs, F. Gerschuetz, L. Hildebrandt, J. Koeth, DFB Lasers between 760 nm and 16 μm for Sensing Applications, Sensors 10 (2010) 2492-2510.
[4] J. E. Dickens, M. S. Vaughn, M. Taylor, M. Ponstingl, An LED array-based light induced fluorescence sensor for real-time process and field monitoring, Sen. Actuators B Chem. 158 (2011) 35-42.
[5] K. Ruxton, A. L. Chakraborty, W. Johnstone, M. Lengden, G. Stewart, K. Duffin, Tunable diode laser spectroscopy with wavelength modulation: Elimination of residual amplitude modulation in a phasor decomposition approach, Sen. Actuators B Chem. 150 (2010) 367-375.
[6] T. Asakawa, N. Kanno, K. Tonokura, Diode laser detection of greenhouse gases in the near-infrared region by wavelength modulation spectroscopy: Pressure dependence of the detection sensitivity, Sensors 10 (2010) 4686-4699.
[7] K. Ruxton, A. L. Chakraborty, W. Johnstone, M. Lengden, G. Stewart, K. Duffin, Tunable diode laser spectroscopy with wavelength modulation: Elimination of residual amplitude modulation in a phasor decomposition approach, Sen. Actuators B Chem. 150 (2010) 367-375.
[8] Tokura, M. Asobe, K. Enbutsu, T. Yoshihara, S. N. Hashida, H. Takenouchi, Real-Time N2O Gas Detection System for Agricultural Production Using a 4.6-μm-Band Laser Source Based on a Periodically Poled LiNbO3 Ridge Waveguide, Sensors 13 (2013) 9999-10013.
[9] A. Upadhyay, A. L. Chakraborty, Residual Amplitude Modulation Method Implemented at the Phase Quadrature Frequency of a 1650-nm Laser Diode for Line Shape Recovery of Methane, IEEE Sens. J. 15 (2015) 1153-1160.
[10] X. Chao, J. B. Jeffries, R. K. Hanson, Absorption sensor for CO in combustion gases using 2.3 μm tunable diode lasers, Meas. Sci. Technol. 20 (2009) 115201-115209.
[11] K. Owen, A. Farooq, A calibration-free ammonia breath sensor using a quantum cascade laser with WMS 2f/1f, Appl. Phys. B 116 (2014) 371-383.
[12] E. D. Tommasi, G. Casa, L. Gianfrani, An intensity-stabilized diode-laser spectrometer for sensitive detection of NH3, Instrum. Meas., IEEE Trans. 56 (2007) 309-312.
[13] L. S. Rothman, D. Jacquemart, A. Barbe, D. C. Benner, M. Birk, L. R. Brown, M.R. Carleer, Jr. C. Chackerian, K. Chance, L.H. Coudert, V. Dana, V. M. Devi, J.-M. Flaud, R. R. Gamache, A. Goldman, J.-M. Hartmann, K.W. Jucks, A. G. Maki, J.-Y. Mandin, S.T. Massie, J. Orphal, A. Perrin, C.P. Rinsland, M.A.H. Smith, J. Tennyson, R.N. Tolchenov, R.A. Toth, J. Vander Auwera, P. Varanasi, G. Wagner, The HITRAN 2004 molecular spectroscopic database, J. Quant. Spectrosc. Radiat. Transfer 96 (2005) 139-204.